DOI: 10.21062/mft.2026.023 http://www.journalmt.com

Process Parameter Effects on Cutting Efficiency and Specific Energy in Abrasive Water Jet Machining

Lianhuan Guo (0009-0001-5565-4912)*[1], Teng Ma (0009-0007-0732-2407)[2], Jin Lan (0009-0002-7437-0840)[3]
[1]Engineering Agency Management Office, Beijing 100032, China. E-mail: glhshenlan@163.com
[2]Engineering Quality Supervision Station of Unit 93121, Dongcheng District, Beijing 100009, China. E-mail: yuwearfeng@yeah.net
[3]CNPC Offshore Engineering Company Limited, Chaoyang District, Beijing 100028, China. E-mail: wenqingzhihe@yeah.net

The manufacturing industry generally focuses on cutting efficiency and specific cutting energy, but existing research on abrasive water jet (AWJ) machining mostly limits itself to one-sided discussions of cutting depth or material removal rate, with few comprehensive and systematic studies on cutting efficiency E and specific cutting energy E_S. To achieve optimal AWJ cutting performance, this paper employs single-factor experiments combined with quantitative calculations and numerical analysis to further investigate the effects of process parameters on cutting efficiency and specific energy. It innovatively reveals the variation patterns of specific cutting energy under different working conditions and determines the parameter values and ranges that maximize cutting efficiency or minimize specific cutting energy. The results show that the minimum specific cutting energy is achieved when the pump pressure reaches three times the threshold pressure, the traverse speed is 110 mm/min, the cutting angle is 90°, the focusing tube diameter is 1.2 mm, and the abrasive mass flow rate is near its optimal value. The influence of standoff distance on specific cutting energy requires comprehensive consideration of both cutting depth and kerf width. Repeated cutting is unfavorable for reducing specific energy, to save energy consumption, single-pass full penetration of the material should be realized whenever possible. This study, aimed at improving AWJ machining efficiency, provides effective research support for achieving high-efficiency and energy-saving cutting processes.

Keywords: Abrasive water jet cutting, Specific cutting energy, Cutting efficiency, Process parameter optimization, Energy consumption

1 Introduction

During maintenance, renovation, and expansion of in-service oil depots (stations), cutting operations involving oil storage tanks and process pipelines are commonly required. However, conventional mechanical cutting methods inevitably generate heat and even open flames [1-4]. Since oil storage equipment and oil pipelines often contain residual oil and oil vapors, conventional thermal cutting methods clearly fail to meet the safety requirements for cutting operations and pose serious safety hazards in oil depot areas. Therefore, abrasive water jet (AWJ) cutting technology, characterized by high energy and cold cutting properties, has attracted significant attention for safe cutting applications [5-7]. For above applications like oil depot facility cutting, the core goal is to safely and rapidly remove large volumes of material, enabling energy-efficient, high-performance cutting operations.

Wang [8-10] acquired generalized AWJ cutting mathematical models. Yu et al. [11] utilized numerical simulation method to obtain single particle acceleration process by SPH coupled FEM. Junkar et al. [12] , Kumar and Shukla [13] and Eltobgy et al. [14] created a finite element analysis of particle impact in AWJ machining. Shahverdi et al. [15] used SPH and ALE methods to simulate AWJ cutting process. However, AWJ cutting performance involves numerous parameters that exhibit complex nonlinear interrelationships [16-20]. Mathematical models and simulation method necessitate the adoption of various simplifying assumptions, which unavoidably result in discrepancies from real-world conditions and difficulties in application.

Fard et al. [21] conducted a comprehensive review summarizing the process fundamentals, material removal mechanisms, and application scenarios, with emphasis on the influence of key micro-abrasive water jet parameters on material removal rate (MRR) and workpiece surface roughness, offering guidance for experimental research on abrasive water jets. Llanto et al. [22] found that increasing water jet pressure and abrasive mass flow rate resulted in lower surface roughness and higher material removal rate for austenitic stainless steel 304L, whereas increasing

traverse speed led to higher surface roughness. The optimal parameters for enhancing material removal rate were a pressure of 300 MPa, a traverse speed of 150 mm/min, and an abrasive mass flow rate of 500 g/min. Uthayakumar et al. [23] evaluated the effects of process parameters via material removal rate and identified water jet pressure as the most influential factor on material removal morphology and surface quality. They reported that excellent surface quality could be achieved when advanced composite material was processed using a high jet pressure of 260 MPa with a moderate feed speed. Rowe et al. [24] investigated the effects of water pressure and traverse speed on the surface roughness of thick carbon fiber reinforced polymer (CFRP) panels and concluded that while increasing water pressure generally improves surface roughness, excessive pressure may exacerbate surface damage. Karthik et al. [25] examined the effects of water jet pressure, traverse speed, and abrasive mass flow rate on the removal rate of 304 stainless steel, the results of which indicated higher removal rates at elevated water pressures and traverse speeds. Nag et al. [26] reported that erosion reaches a maximum at a certain standoff distance; further increases in standoff distance reduce erosion capability, with no visible erosion beyond a specific threshold. Lissek [27]、Sharma [28]、Nag [29] have studied the influence of process parameters on different materials, covering a variety of materials from metals and composites to ceramics and polymers, based on their results, material-cutting efficiency depends not only on individual parameters but also on their combined effects. Ganovska et al. [30] focused on the application of an artificial neural network model for surface roughness prediction, and solved the problem of the systematic monitoring and control of the abrasive water jet cutting process. Lei [31], Yang [32] also successfully predicted the abrasive water jet cutting quality using artificial neural networks. Hreha et al. [33] analyzed acoustic emission recorded during monitoring of abrasive waterjet cutting of stainless steel AISI 309, and achieved good surface roughness control.

However, the aforementioned experimental studies have limitations and tend to be narrowly focused. Most of them merely analyze the effects of process parameters on material removal rate or surface roughness without taking into account energy consumption during cutting, which is inconsistent with the economic considerations of cutting operations. For instance, it entails substantial energy costs to enhance material removal rate and surface quality by increasing pump pressure or to minimize surface roughness by reducing traverse speed and increasing the number of cutting passes. Consequently, the energy required to remove a unit volume of material becomes relatively high, i.e. the specific cutting energy E_S is elevated. Moreover, there are no specific discussions about the influence of abrasive mass flow rate, focusing tube inner diameter, and standoff distance on specific cutting energy remains unexplored. This paper intends to employ a single-factor experimental approach to systematically calculate and analyze the effects of pump pressure, traverse speed, cutting angle, focusing tube diameter, abrasive mass flow rate, standoff distance, and the number of cutting passes on cutting efficiency E and specific cutting energy E_S , thereby identifying the optimal process parameters and ranges conducive to energy-efficient, high-speed cutting.

2 Experimental Platform Setup

To evaluate the efficacy of high-pressure AWJ cutting on X60 pipeline steel, an AWJ cutting system was designed and constructed. Figs. 1(a)-(b) show the schematic diagrams of the high-pressure AWJ cutting system, and Figs. 2(a)-(d) show photographs of the apparatus.

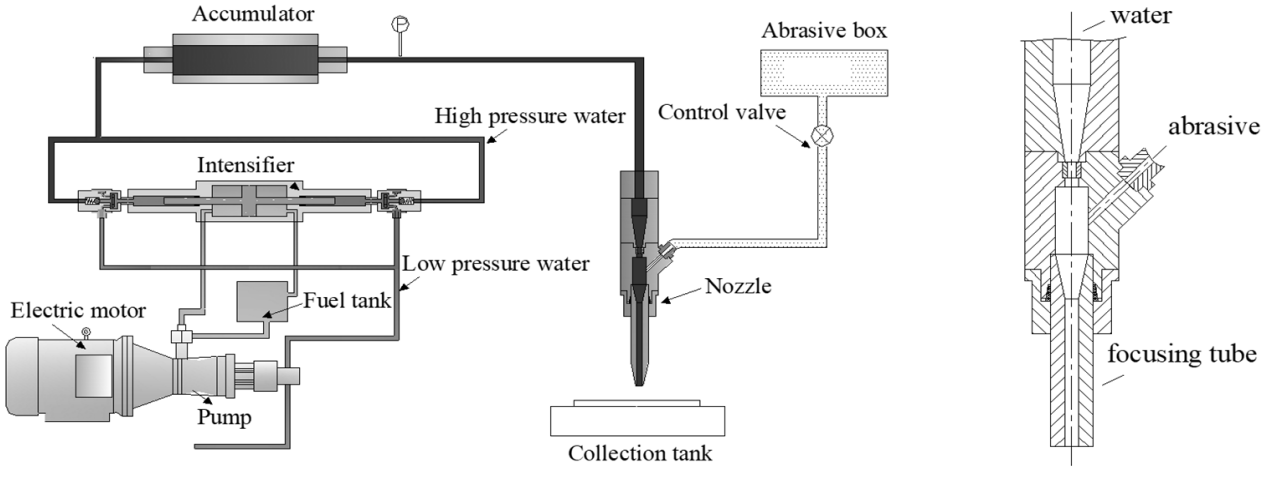

Fig. 1 *Schematic diagrams of the high-pressure AWJ cutting system*

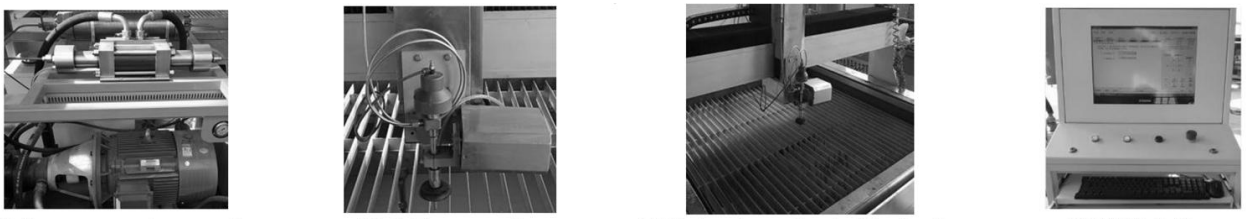
(a) High-pressure water generation (b) Cutting execution (c) Wastewater and material collection (d) CNC platform

Fig. 2 *Photographs of the apparatus*

The experimental equipment employs a high-pressure AWJ cutting system based on post-mixing. In this system, the abrasive is added via a post-mixing method, and the abrasive mass flow rate can be adjusted through a regulating valve. The main technical parameters of the system are presented in Tab 1.

Tab. 1 *Main technical parameters of the AWJ cutting system*

Technical Parameter	Numerical Range
Jet pressure (p)	0-380MPa
Maximum water flow rate (q_w)	3.7L/min (at 380 MPa)
Abrasive mass flow rate (m_a)	0-16g/s
Traverse speed (v)	0-1m/min
Water nozzle diameter (d_0)	0.3mm
Focusing tube diameter (d)	0.5-1.5mm
Standoff distance (s)	0-150mm

3 Experimental Results and Analysis

Fig. 3 shows the experimental samples of X60 pipeline steel cut by high-pressure AWJ. Following the cutting process, the samples were sequentially labeled in accordance with the experiment number. Compressed air guns were employed to blow out abrasive particles trapped in the kerfs, which helped maintain a dry environment inside the kerfs and prevented rusting of the samples after cutting, thus avoiding any impact on the measurement of experimental results.

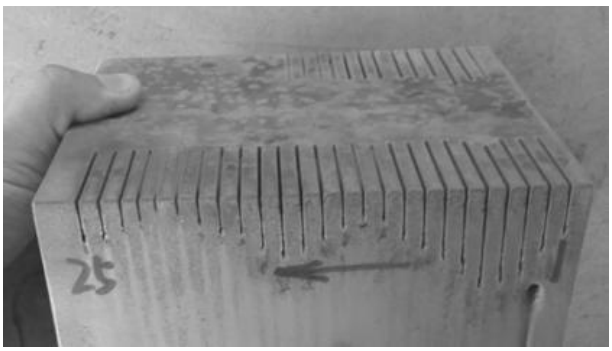

Fig. 3 *Experimental samples*

3.1 Effect of Pump Pressure on Cutting Performance

Experimental parameters: Pump pressure 150-310 MPa, traverse speed 50-170 mm/min, focusing tube diameter 0.5-1.5 mm, abrasive mass flow rate 2.1-15.3 g/s, standoff distance 4 mm, cutting angle 90°, and number of passes 1.

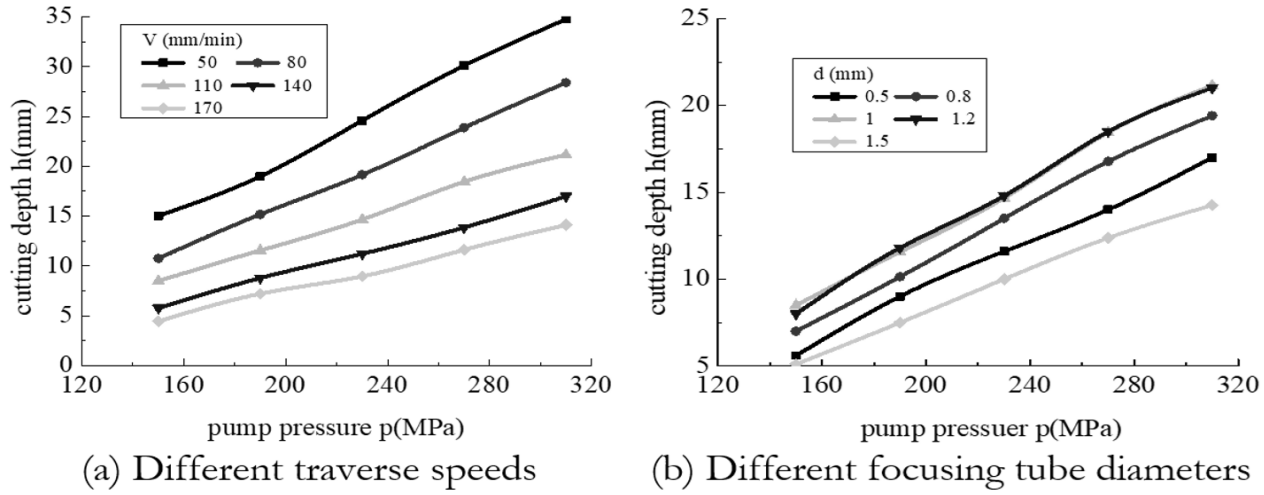

Fig. 4 *Relationship curve between cutting depth and pump pressure*

Figs. 4(a)-(b) show the relationship between pump pressure and cutting depth. An increase in pump pressure corresponds with a progressive increase in cutting depth. Given that the traverse speed is held constant, the cutting efficiency E similarly exhibits an upward trend. Nevertheless, the enhancements in

cutting depth and efficiency are accompanied by elevated energy consumption by the equipment and do not indicate a linear increase in specific cutting energy. After acceleration through the water nozzle, the high-pressure water forms a high-speed water jet. In accordance with Bernoulli's equation:

$$p_{at} + \frac{\rho_w}{2} \cdot v_0^2 + \rho_w \cdot g \cdot h_1 = p + \frac{\rho_w}{2} \cdot v_{pipe}^2 + \rho_w \cdot g \cdot h_2 \quad (1)$$

Since atmospheric pressure $p_{at} << p$, $h_1 = h_2$, and $v_0 >> v_{pipe}$, the velocity of the water jet after the nozzle v_0 is:

$$v_0 = \mu \cdot \sqrt{\frac{2 \cdot p}{\rho_w}} \quad (2)$$

Of which the flow coefficient μ represents momentum losses attributable to wall friction, turbulent flow, and water compressibility. This coefficient exhibits an approximately linear decline as pump pressure increases, resulting in the water jet velocity v_0 not rising linearly with pump pressure but rather demonstrating a progressively diminishing rate of increase. The economic efficiency of AWJ cutting is assessed by the specific cutting energy E_S, which refers to the energy consumed to cut a unit volume of material, i.e., $E_S = E_A/V_m$, where E_A represents the AWJ energy consumption required to cut a material volume V_m. To achieve optimal economy, E_S should be minimized.

$$\begin{cases} E_A = \frac{1}{2} \cdot m_A \cdot V_A^2 \cdot t \\ m_A = \frac{\pi}{4} \cdot d_0^2 \cdot v_0 \cdot \rho_A \end{cases} \quad (3)$$

From Eqs. (2) and (3), it can be derived that $E_A \propto p^{1.5}$. Where $V_m = h \cdot b \cdot L = h \cdot b \cdot v \cdot t$(b and L represent kerf width and length, respectively, which are independent of p). In accordance with the existing experimental data, the cutting depth h and the pump pressure p have the following relationship, which is consistent with the results proposed by Hashish [34]:

$$h = C \cdot (p - p_{th}) \quad (4)$$

Of which C is a proportionality constant and p_{th} is the threshold pressure. Assuming kerf width is constant, then $V_m \propto (p\text{-}p_{th})$. If E_S takes the minimum value, then it requires:

$$\frac{dE_A}{dV_m} = \frac{d(C_1 \cdot p^{1.5})}{d(C_2 \cdot (p - p_{th}))} = 0 \quad (5)$$

The solution to Eq. (5) is $p = 3p_{th}$, meaning that when the pump pressure is three times the threshold pressure, E_S is minimized, resulting in the highest energy efficiency for material cutting. Thus, specific cutting energy E_S is closely related to the threshold pressure. The threshold pressure of the material is not fixed; it changes with process parameters. Figs 5(a)-(b) show the effects of traverse speed v and focusing tube diameter d on threshold pressure p_{th}, respectively. The results indicate that the threshold pressure rises as the traverse speed increases, while it initially decreases and subsequently increases with the enlargement of the focusing tube diameter.

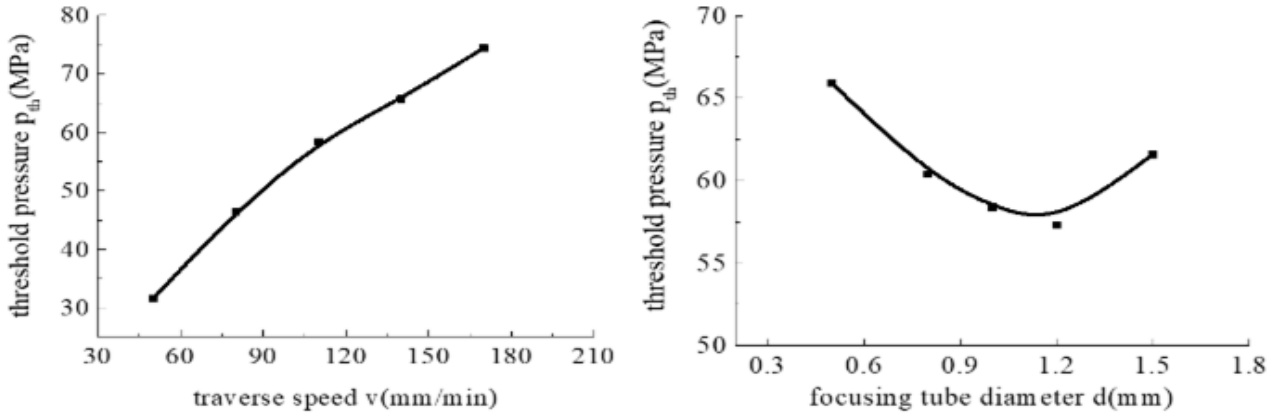

(a) Threshold pressure at different traverse speeds

(b) Threshold pressure at different focusing tube diameters

Fig. 5 *Curves of threshold pressure variation with process parameters*

From the obtained threshold pressures, the cutting pressure corresponding to the lowest specific cutting energy can be determined as $3p_{th}$. At traverse speeds of 50 mm/min, 80 mm/min, 110 mm/min, 140 mm/min, and 170 mm/min, the cutting pressures corresponding to the lowest specific cutting energy are

94.8 MPa, 139.2 MPa, 175.2 MPa, 197.1 MPa, and 223.2 MPa, respectively. At focusing tube diameters of 0.5 mm, 0.8 mm, 1.0 mm, 1.2 mm, and 1.5 mm, the cutting pressures corresponding to the lowest specific cutting energy are 197.7 MPa, 181.2 MPa, 175.2 MPa, 171.9 MPa, and 184.8 MPa, respectively.

3.2 Effect of Traverse Speed on Cutting Performance

Among many factors, nozzle traverse speed is the only one closely related to cutting time, reflecting the duration of AWJ impact on the material. Experimental parameters: traverse speed 50-170 mm/min, pump pressure 150-310 MPa, focusing tube diameter 1 mm, abrasive mass flow rate 2.1 g/s, standoff distance 4 mm, cutting angle 90°, and number of passes 1.

Fig. 6 shows the relationship between traverse speed v and cutting depth h. After curve fitting, the mathematical expression can be written in the form $h=c\cdot v^{k}$, where c and k are constants, with k being negative and ranging from -0.7 to -1, consistent with the law summarized by Momber [35]. As the traverse speed increases, the cutting depth decreases, but the rate of decrease gradually slows down. Taking the cutting depth variation curve at 310 MPa as an example, within the speed range of 50-110 mm/min, the cutting depth decreases significantly, dropping from 15 mm to 8.5 mm, a reduction of about 7 mm. When the traverse speed further increases, the decrease in cutting depth is not obvious; in the speed range of 110-170 mm/min, the cutting depth tends to stabilize around a certain value, decreasing from about 8 mm to 4.5 mm, a reduction of only about 3.5 mm.

An increase in traverse speed directly results in shallower cutting depth; however, this does not imply that slower nozzle traverse speeds are inherently more advantageous. Excessively slow traverse speeds can adversely impact cutting efficiency. Fig. 7 shows the relationship curve between AWJ cutting efficiency and traverse speed. Although the cutting depth decreases with an increase in traverse speed, Fig. 7 indicates that cutting efficiency E does not follow the same decreasing trend. Instead, it first increases and then decreases, indicating the existence of an optimal traverse speed within the experimental parameters that maximizes cutting efficiency. Meanwhile, the figure shows that under different pressure conditions, the optimal traverse speed is around 110 mm/min, where the cutting efficiency peaks. The traverse speed range of 50-110 mm/min corresponds to the rising zone of the cutting efficiency, while the traverse speed range of 110-170 mm/min corresponds to the declining zone of the cutting efficiency. Under these experimental conditions, the trend of specific cutting energy is inversely related to the cutting efficiency. At the same energy consumption, when the traverse speed is 110 mm/min, the AWJ can remove a larger volume of material, and the specific cutting energy E_S reaches its minimum value.

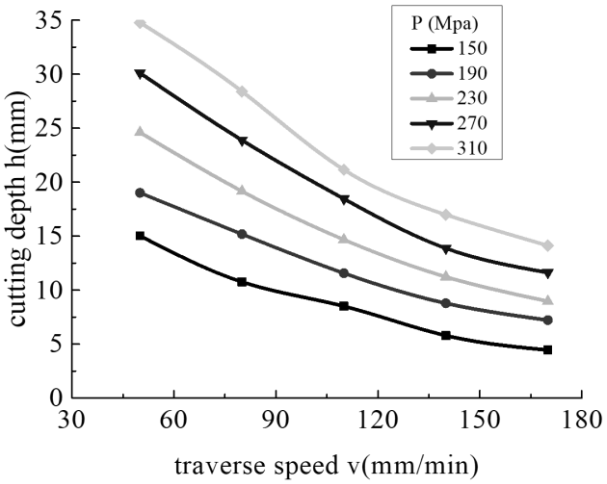

Fig. 6 *Relationship curve between cutting depth and traverse speed*

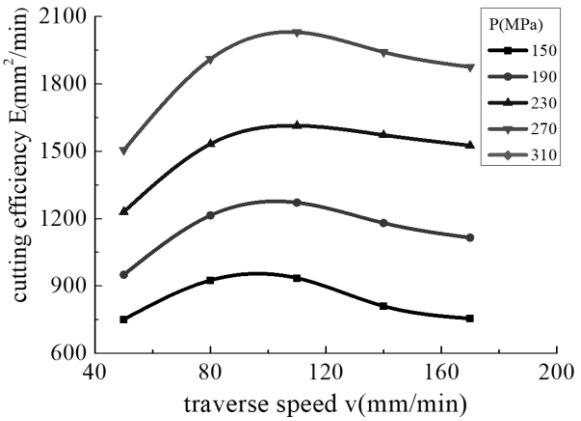

Fig. 7 *Relationship curve between cutting efficiency and traverse speed*

3.3 Influence of Standoff Distance on Cutting Performance

The standoff distance refers to the distance from the water jet nozzle exit to the material being cut. As an important factor affecting water jet cutting performance, increasing the standoff distance significantly changes the jet's structure and velocity. Experimental parameters: Standoff distance 1-13 mm, traverse speed 50-170 mm/min, pump pressure 150-310 MPa, focusing tube diameter 1 mm, abrasive mass flow rate 2.1 g/s, cutting angle 90°, and number of passes 1.

The relationship curve between standoff distance and cutting depth under non-submerged conditions is shown in Fig. 8. Under certain conditions, as the standoff distance increases, the cutting depth first increases and then decreases. There is an optimal jet standoff distance near 4 mm where the cutting depth reaches its maximum. When the standoff distance continues to increase beyond 4 mm, the cutting depth

decreases. The main reason for this phenomenon is: when the standoff distance is less than 4 mm, due to the short distance between the nozzle and the target, abrasive particles are not fully accelerated by the water jet, so their kinetic energy upon impacting the target material is still relatively low. Additionally, the fluid reflected after impacting the target significantly affects the subsequent flow; this reflected fluid causes the water jet to diverge and weakens its impact velocity, dissipating part of the water jet's kinetic energy before it reaches the target surface. When the standoff distance exceeds 4 mm and continues to increase, the entrainment of air significantly affects the jet velocity. According to the water jet characteristic diagram described by Japanese scholars Yanaida and Ohashi, as the jet exits the nozzle, it exchanges mass and momentum with the surrounding medium. With increasing distance from the abrasive nozzle, the jet diffuses, with diffusion developing from the surface toward the jet core, axial dynamic pressure decreases, cutting ability declines, and cutting depth reduces. Fig. 9 illustrates the jet divergence phenomenon.

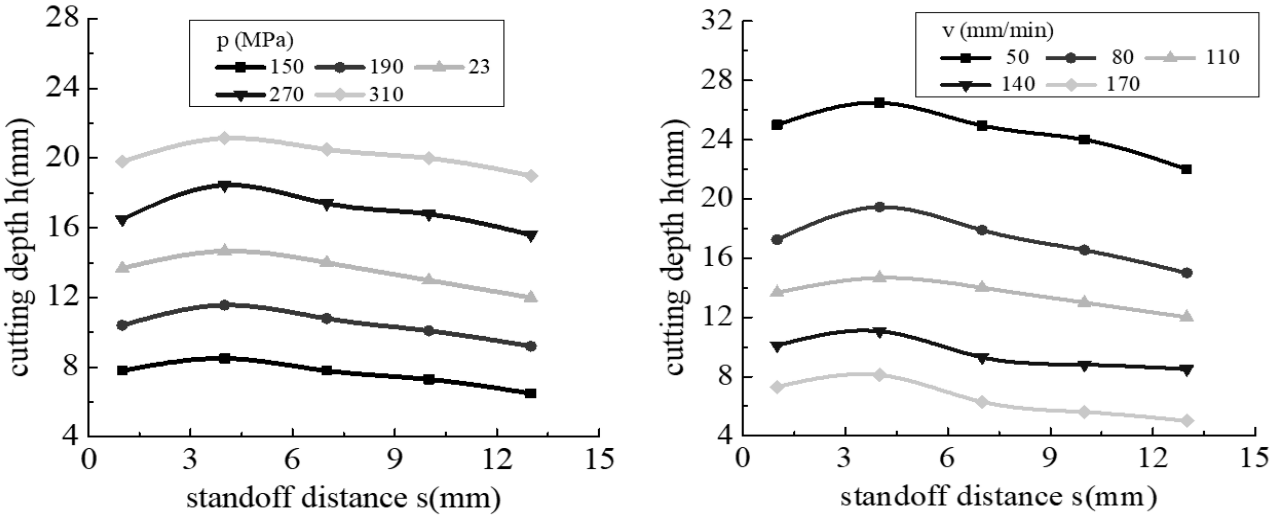

(a) Relationship curve between cutting depth and standoff distance under different pump pressures

(b) Relationship curve between cutting depth and standoff distance under different traverse speeds

Fig. 8 *Relationship curve between cutting depth and standoff distance*

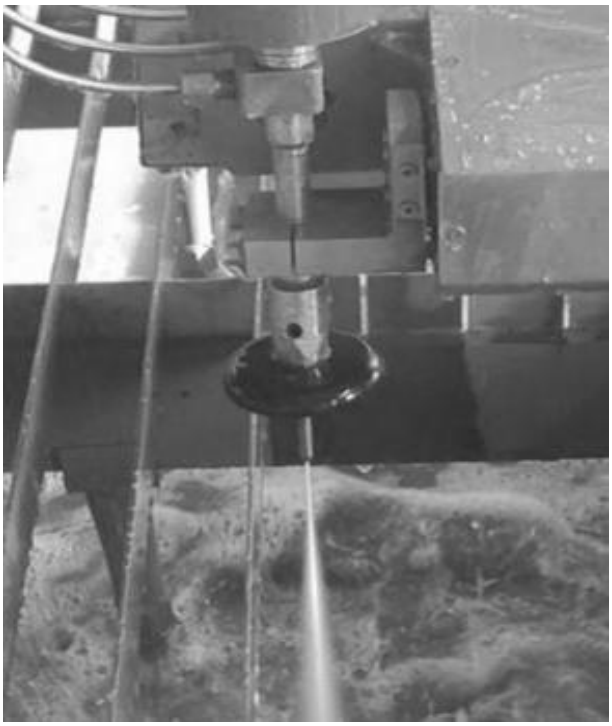

Fig. 9 *Jet divergence phenomenon*

Under the experimental conditions, the cutting efficiency can be directly assessed by comparing cutting depths: The greater the cutting depth, the higher the cutting efficiency at the corresponding standoff distance. However, changes in the standoff distance also affect kerf width. At small standoff distances (s<4mm), both cutting depth and kerf width increase with increasing standoff distance, and the specific cutting energy tends to decrease. At larger standoff distances (s>4mm), although cutting depth decreases somewhat, the increase in kerf width may result in an overall increase in the volume of material removed. In other words, the specific cutting energy at large standoff distances does not necessarily increase. The influence of the standoff distance on the specific cutting energy must consider both cutting depth and kerf width comprehensively.

3.4 Influence of Cutting Angle on Cutting Performance

When AWJ are operated on-site, due to operational constraints and actual cutting requirements, the nozzle often needs to cut at a certain

inclination angle. In this study, the cutting angle is defined as the angle between the nozzle centerline and the direction of traverse speed. Figs 10(a)-(e) show the cutting angles adjusted during the experiments, which are 40°, 65°, 90°, 115°, and 140°, respectively. Experimental parameters: Cutting angle 40°-140°, standoff distance 1-13 mm, traverse speed 50-170 mm/min, pump pressure 230 MPa, focusing tube diameter 1 mm, abrasive mass flow rate 2.1 g/s, and number of passes 1.

As shown in Figs 11(a) and 12(b), the relationship between cutting angle and cutting depth exhibits a parabolic shape. When the cutting angle is less than 90°, the cutting depth increases with the angle, reaching a maximum at 90°. When the angle exceeds 90°, the cutting depth decreases. This phenomenon occurs because at smaller cutting angles, the vertical component of the water jet's impact velocity on the target is smaller, reducing the fluid's erosive kinetic energy on the target. Although the fluid after cutting continues to scour the formed kerf at a certain velocity, achieving a similar effect to repeated cutting, the reduction in vertical velocity component has a more significant impact, leading to decreased cutting depth. When the cutting angle exceeds 90°, not only does the vertical velocity component decrease, but the increased impact angle also strengthens the jet reflection effect, which offsets part of the jet's impact capability.

Under these experimental conditions, the cutting efficiency follows the same trend as the cutting depth, no detailed plot of cutting efficiency will be provided here, and the minimum specific cutting energy occurs at the operating condition with the highest cutting efficiency.

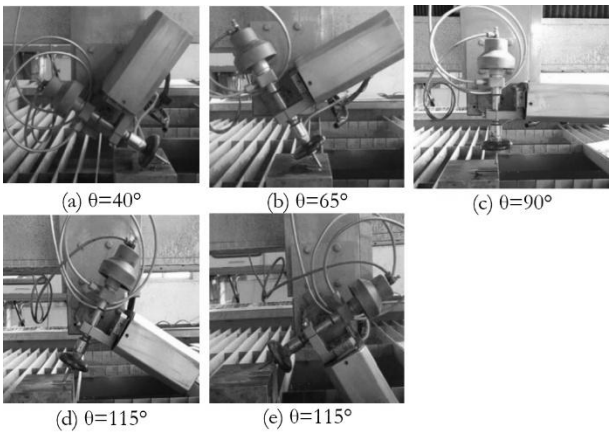

Fig. 10 *Different cutting angles in the experiment*

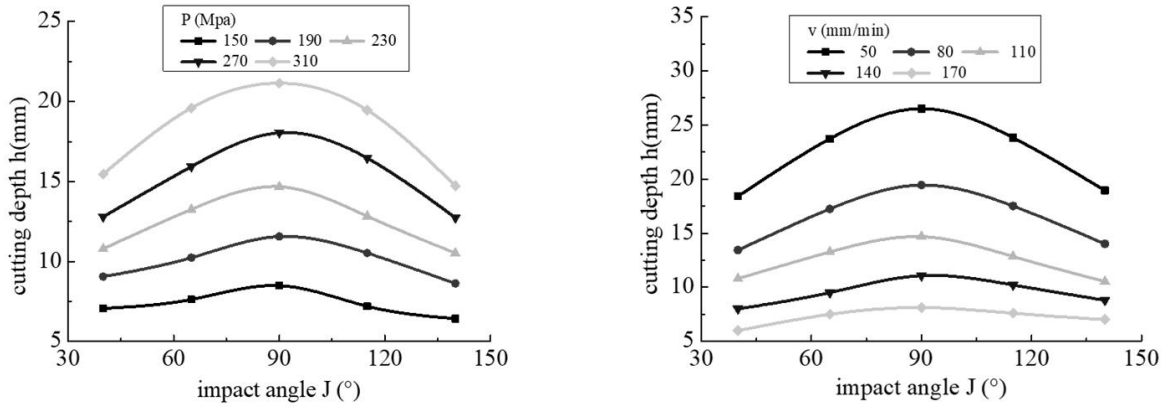

(a) Relationship between cutting depth and cutting angle under different pump pressures

(b) Relationship between cutting depth and cutting angle under different traverse speeds

Fig. 11 *Relationship curve between cutting depth and cutting angle*

3.5 Influence of Abrasive Mass Flow Rate on Cutting Performance

When the abrasive particle size in the AWJ is fixed, the abrasive mass flow rate reflects the number of abrasive particles in the jet, which directly affects the frequency of impact on the material and thus influences the cutting depth. Experimental parameters: Abrasive mass flow rate 2.1-15.3 g/s, pump pressure 150-310 MPa, traverse speed 110 mm/min, standoff distance 4 mm, focusing tube diameter 1-1.5 mm, cutting angle 90°, and number of passes 1.

Fig. 12 shows the relationship curve between the abrasive mass flow rate and the cutting depth. The relationship can be expressed in a form of $h = k \cdot m_a^n$,where k is a constant and n is a function of the mass flow rate: When the abrasive flow rate is at a low level, the exponent n = 1, indicating an approximately linear relationship between the cutting depth and the mass flow rate; when the abrasive flow rate increases to a certain value, the cutting depth reaches a maximum; thereafter, as the abrasive flow rate continues to increase, the cutting depth begins to decrease, with n<0. Therefore, under fixed cutting conditions, there is an optimal range of abrasive mass flow rate that maximizes cutting depth. The reason for the above phenomenon can be explained as follows: when the abrasive mass flow rate is low, increasing the mass

flow rate increases the number of abrasive particles emitted per unit time, raising the frequency of abrasive impacts on the target material and thus increasing the cutting depth. However, when the mass flow rate reaches a certain value, further increases cause significant interactions among abrasive particles inside the nozzle. Collisions between particles can blunt particle edges or even cause particle breakage, reducing the number of effective abrasive particles impacting the target. Although the number of particles increases, the average kinetic energy per particle decreases, leading to a reduction in the total kinetic energy of the jet, weakening the abrasive jet's erosive ability on the material. Therefore, in this stage, increasing the abrasive mass flow rate actually reduces the cutting depth, showing a downward trend in the curve.

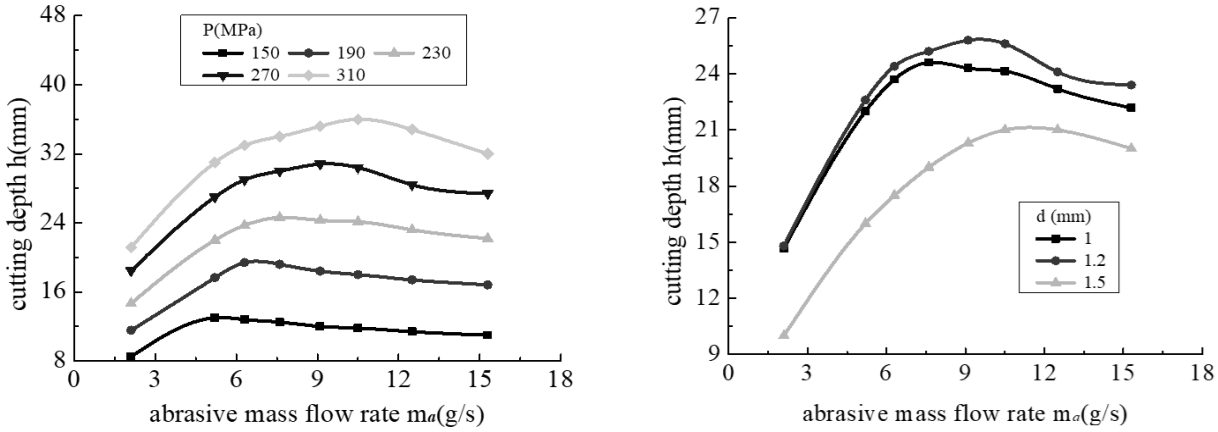

(a) Curves of mass flow rate versus cutting depth under different pump pressures

(b) Curves of mass flow rate versus cutting depth under different focusing tube diameters

Fig. 12 *Relationship curves between abrasive mass flow rate and cutting depth*

Given that the abrasive mass flow rate significantly affects the cutting depth, selecting it reasonably can effectively reduce abrasive consumption while better ensuring the quality of the cut surface and cutting efficiency. Thus, it is necessary to set the abrasive mass flow rate appropriately in practical engineering applications and manufacturing processes. Figs 13(a)-(b) show the optimal mass flow rate curves under different pump pressures and focusing tube diameters, respectively. The corresponding flow rates yield the maximum cutting depth.

The curve of cutting efficiency versus abrasive mass flow rate is similar to that of cutting depth versus mass flow rate. Comparing Fig. 12(a) and Fig. 14, it can be seen that at 230 MPa, both cutting efficiency and cutting depth reach their maximum values at the optimal mass flow rate of 7.6 g/s, while the specific cutting energy reaches its minimum near this optimal mass flow rate.

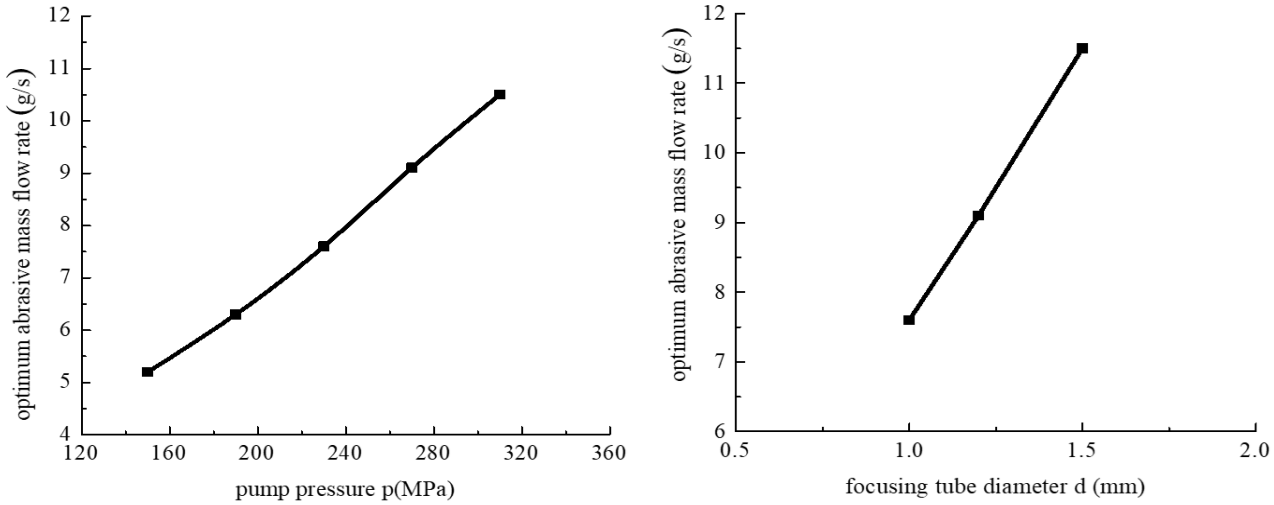

(a) Optimal mass flow rate under different pump pressures

(b) Optimal mass flow rate under different focusing tube diameters

Fig. 13 *Optimal abrasive mass flow rate curves*

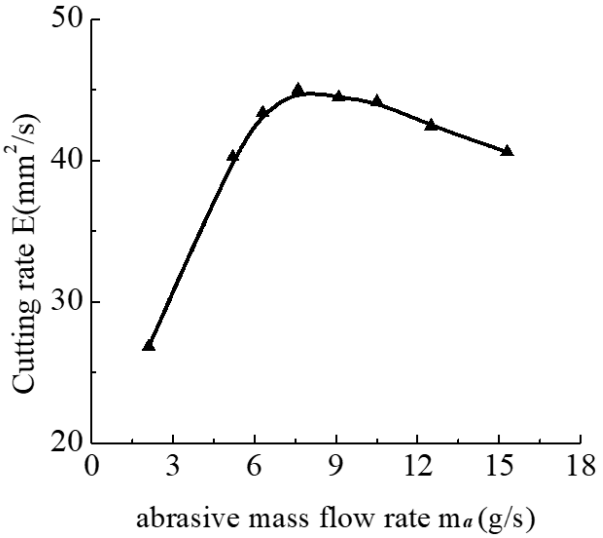

Fig. 14 *Cutting efficiency of different mass flow rate*

3.6 Influence of Nozzle Diameter on Cutting Performance

The nozzle diameter not only affects the jet flow rate, but also influences the mixing and acceleration of abrasive particles with water. The nozzle diameter is not inherently superior when smaller or larger. Instead, there exists an optimal value at which the acceleration performance of the AWJ is maximized. Experimental parameters: Nozzle diameter 0.5-1.5 mm, pump pressure 150-310 MPa, traverse speed 110 mm/min, abrasive mass flow rate 2.1 g/s, standoff distance 4 mm, cutting angle 90°, and number of passes 1.

Experimental results show that the maximum cutting depth is achieved when the focusing tube diameter is in the range of 1-1.2 mm, while the water nozzle diameter is 0.3 mm. This is consistent with many literature reports that the optimal focusing tube diameter is 3-4 times the water nozzle diameter. The influence of different focusing tube diameters on the cutting depth is shown in Fig. 15. The trend of cutting efficiency changes with nozzle diameter is consistent with that of the cutting depth, while the variation of specific cutting energy is similar to that described in Section 3.3. Changing the nozzle diameter also affects the kerf width. For small focusing tube diameters (df<1.2mm), both cutting depth and kerf width increase as the nozzle diameter increases, and specific cutting energy shows a decreasing trend. For large focusing tube diameters (df>1.2mm), although cutting depth decreases to some extent, the increase in kerf width may still increase the volume of material removed. In other words, specific cutting energy does not necessarily increase with large focusing tube diameters. The influence of nozzle diameter on specific cutting energy E_S must also consider both cutting depth and kerf width comprehensively. As shown in Fig. 15, at 190 MPa pressure, the cutting depth with a 1 mm diameter nozzle is 11.5 mm, while with a 1.4 mm diameter nozzle, the cutting depth is only 8.9 mm. Although the cutting depth decreases significantly, due to the substantial increase in kerf width, the material removal rate under the same energy consumption actually increases. Fig. 16 shows that when the focusing tube diameter is 1.2 mm, the material removal rate is maximized, i.e., the specific cutting energy E_S is minimized.

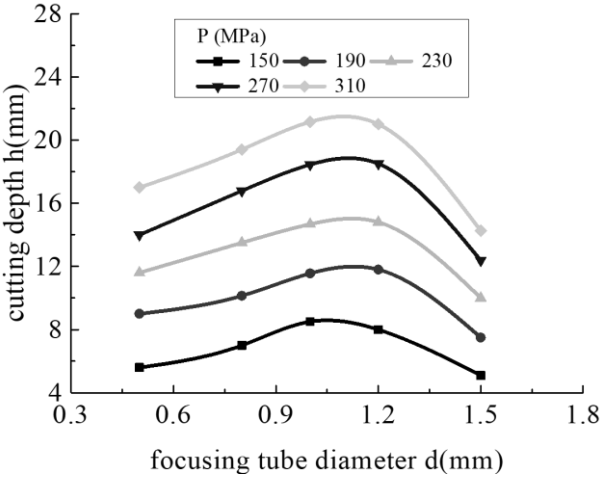

Fig. 15 *Relationship between cutting depth and focusing tube diameter*

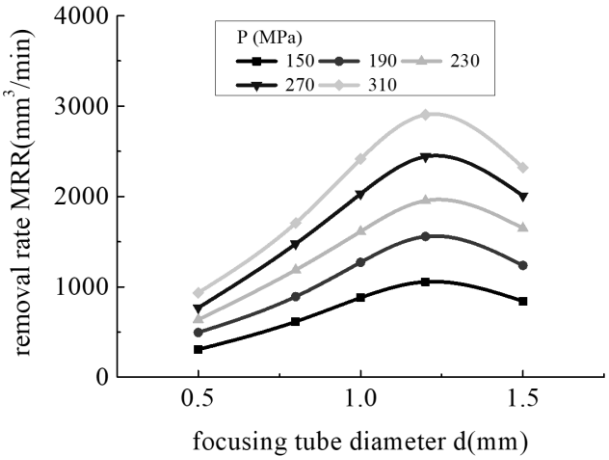

Fig. 16 *Relationship between focusing tube diameter and MRR*

3.7 Influence of Repeated Cutting on Cutting Performance

In engineering applications, AWJ cutting often cannot penetrate the material in a single pass, requiring repeated cutting. In this case, the relationship between the number of repeated cutting, cutting depth, and specific cutting energy must be considered. Experimental parameters: Number of passes 1-6, nozzle diameter 1 mm, pump pressure 230 MPa, traverse speed 110 mm/min, abrasive mass flow rate 2.1 g/s, standoff distance 4 mm, and cutting angle 90°.

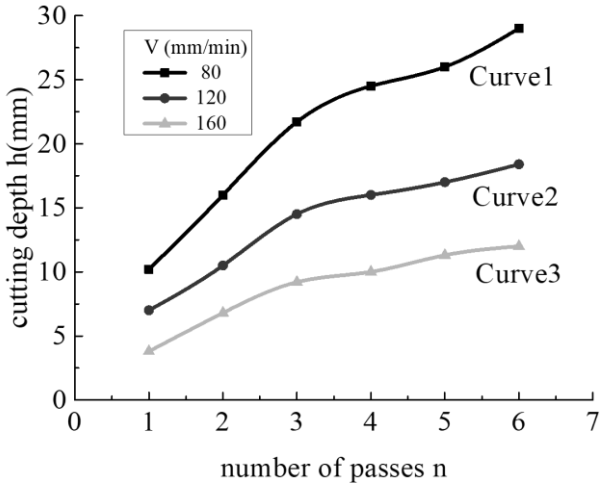

Fig. 17 *Relationship curve between cutting depth and number of passes*

In Fig. 17, curve 1 shows the relationship between the number of repeated cutting and cutting depth at a traverse speed of 80 mm/min, exhibiting a trend of continuously decreasing growth rate in cutting depth. At the same traverse speed, cutting twice consumes twice the energy, but curve 1 in Fig. 17 shows that the depth after two cuts is far less than twice that of a single cut, meaning the specific cutting energy E_S for repeated cutting is higher, which is unfavorable for reducing energy consumption. Curve 2 and curve 3 show the same pattern. This phenomenon can be explained as follows: as cutting depth increases, the actual standoff distance of the AWJ increases, friction losses caused by the kerf walls increase, and the accumulation of the water cushion layer inside the kerf causes a sharp loss of AWJ energy. Comparing cutting depths under the same energy consumption, a single cut at 80 mm/min traverse speed achieves a greater depth than two cuts at 160 mm/min within the same time. A greater cutting depth means more material volume removed, which corresponds to a lower specific cutting energy E_S. From curve 1 and curve 3 in the figure, the depth of a single cut at 80 mm/min is greater than that of two cuts at 160 mm/min, both lying on the same energy consumption line, indicating that the specific cutting energy E_S is lower at low-speed single cutting than at high-speed repeated cutting. In summary, repeated cutting is not conducive to reducing specific cutting energy. To lower energy consumption, it is best to achieve full penetration in a single pass.

4 Conclusions

To meet the operational demands of improving cutting efficiency and reducing specific cutting energy in AWJ cutting, this study established a CNC five-axis linkage cutting platform to enable adjustment of various processing parameters and process control. Using a single-factor experimental method, the effects of different process parameters on cutting performance were investigated. Through qualitative mechanism analysis and quantitative calculations, the parameter values and ranges that achieve the highest cutting efficiency E or the lowest specific cutting energy E_S were determined. The results indicate that when the pump pressure reaches three times the threshold pressure, the traverse speed is 110 mm/min, the cutting angle is 90°, the focusing tube diameter is 1.2 mm, and the abrasive mass flow rate is near the optimal value, the specific cutting energy is minimized. The effects of standoff distance on specific cutting energy require careful consideration of both cutting depth and kerf width. Repeated cutting is unfavorable for reducing specific cutting energy, single-pass cutting through the material should be achieved whenever possible to save energy consumption. This study provides theoretical support for achieving efficient and energy-saving cutting processing with AWJ technology.

Further investigation into advanced control systems, such as those incorporating artificial intelligence and machine learning, is needed to improve process accuracy, efficiency, and energy conservation. It will offer a promising avenue to understand and predict complex jet-material interactions with greater fidelity, leading to more robust optimization strategies and balance between enhancing surface quality and controlling energy consumption.

References

[1] WOLF, J., KRUMME, E., BANDARU, N. K., DIENWIEBEL, M., ZABEL, A., MÖHRING, H. C. (2026). A grey-box approach based on Johnson-Cook constitutive model to improve predictions of mechanical loads of cutting simulations for normalized AISI 1045. *CIRP Journal of Manufacturing Science and Technology*, Vol. 65, pp. 163-178.

[2] MILOVANČEVIĆ, M., SPASOV, K. B., RAHIMI, A. (2024). Optimization of the Plasma Arc Cutting Process Through Technological Forecasting. *Journal of Engineering Management and Systems Engineering*, Vol. 3, No. 1, pp. 30-37.

[3] WASZCZUK, K. P. (2024). Influence of technological parameters on the cutting temperature during trochoidal milling. *Manufacturing Technology*, Vol. 24, No. 1, pp. 148–153.

[4] TIAN, H. Q. MA, H. Q. (2023). Modeling and Coefficient Identification of Cortical Bone Milling Forces of Ball-End Milling Cutter for

Orthopaedic Robot. *Journal of Industrial Intelligence*, Vol. 1, No. 4, pp. 229-240.

[5] TIAN, J., LINTAO, L., REN, B., BIAN, G., HUANG, S. (2024). Carbide twist drill spiral groove abrasive flow polishing and abrasive flow analysis. *Manufacturing Technology*, Vol. 24, No. 2, pp. 197–206.

[6] HASHISH, M. (1987). Turning with abrasive-waterjets—a first investigation. *Journal of Engineering for Industry*, Vol. 109, No. 4, pp. 281-290.

[7] LUSI, N., GEBREMARIAM, M., ALAO, A.-R., SAPTAJI, K., AZHARI, A. (2025). Investigation of the wear progression of nozzle in abrasive waterjet machining with different abrasive material. *Manufacturing Technology*, Vol. 25, No. 1, pp. 76–85.

[8] WANG, J. (2009). A new model for predicting the depth of cut in abrasive waterjet contouring of alumina ceramics. *Journal of Materials Processing Technology*, Vol. 209, No. 5, pp. 2314-2320.

[9] WANG, J., GUO, D. M. (2002). A predictive depth of penetration model for abrasive waterjet cutting of polymer matrix composites. *Journal of Materials Processing Technology*, Vol. 121, No. 2-3, pp. 390-394.

[10] WANG, J. (2007). Predictive depth of jet penetration models for abrasive waterjet cutting of alumina ceramics. *International Journal of Mechanical Sciences*, Vol. 49, No. 3, pp. 306-316.

[11] YU, F., WANG, J. M., LIU, F. H. (2012). Numerical simulation of single particle acceleration process by SPH coupled FEM for abrasive waterjet cutting. *The International Journal of Advanced Manufacturing Technology*, Vol. 59, No. 1, pp. 193-200.

[12] JUNKAR, M., JURISEVIC, B., FAJDIGA, M., GRAH, M. (2006). Finite element analysis of single-particle impact in abrasive water jet machining. *International Journal of Impact Engineering*, Vol. 32, No. 7, pp. 1095-1112.

[13] KUMAR, N., SHUKLA, M. (2012). Finite element analysis of multi-particle impact on erosion in abrasive water jet machining of titanium alloy. *Journal of Computational and Applied Mathematics*, Vol. 236, No. 18, pp. 4600-4610.

[14] ELTOBGY, M. S., NG, E., ELBESTAWI, M. A. (2005). Finite element modeling of erosive wear. *International Journal of Machine Tools and Manufacture*, Vol. 45, No. 11, pp. 1337-1346.

[15] SHAHVERDI, H., ZOHOOR, M., MOUSAVI, S. M. (2011). Numerical simulation of abrasive water jet cutting process using the SPH and ALE methods. *International Journal of Advanced Design and Manufacturing Technology*, Vol. 5, No. 1, pp. 43-50.

[16] LENIN, N., KUMAR, S., GUPTA, N. K., KARTHICK, A., SURIYAN, R., PANCHAL, H., SADASIVUNI, K. K. (2023). Experimental analysis and optimization of abrasive waterjet deep hole drilling process parameters for SS AISI 316L. *Journal of Materials Research and Technology*, Vol. 26, pp. 7984-7997.

[17] SRINIVASU, D. S., BABU, N. R. (2008). A neuro-genetic approach for selection of process parameters in abrasive waterjet cutting considering variation in diameter of focusing nozzle. *Applied Soft Computing*, Vol. 8, No. 1, pp. 809-819.

[18] PARIKH, P. J., LAM, S. S. (2009). Parameter estimation for abrasive water jet machining process using neural networks. *The International Journal of Advanced Manufacturing Technology*, Vol. 40, No. 5, pp. 497-502.

[19] CHAKRAVARTHY, S. P., BABU, R. N. (2000). A hybrid approach for selection of optimal process parameters in abrasive water jet cutting. *Proceedings of the Institution of Mechanical Engineers, Part B: Journal of Engineering Manufacture*, Vol. 214, No. 9, pp. 781-791.

[20] ZAIN, A. M., HARON, H., SHARIF, S. (2011). Genetic algorithm and simulated annealing to estimate optimal process parameters of the abrasive waterjet machining. *Engineering with Computers*, Vol. 27, No. 3, pp. 251-259.

[21] FARD, M.,G., NAG, A., PETRU, J., HLOCH,S. (2025). Towards sustainable precision: A review of water jet meso and micromachining. *Results in Engineering*, 27 (2025) 106447.

[22] LLANTO, J. M., A. VAFADAR, A., AAMIR, M., TOLOUEI-RAD, M. (2021). Analysis and optimization of process parameters in abrasive waterjet contour cutting of AISI 304L. *Metals*, Vol. 11, No. 9, pp. 1362.

[23] UTHAYAKUMAR, M., KHAN, M. A., KUMARAN, S. T., SLOTA, A., ZAJAC, J. (2016). Machinability of nickel-based superalloy by abrasive water jet machining. *Mater. Manuf. Process*, Vol. 31, pp. 1733–1739.

[24] ROWE, A., PRAMANIK, A., BASAK, A. K., PRAKASH, C., SUBRAMANIAM, S., DIXIT,

A. R., RADHIKA, N. (2023). Effects of abrasive waterjet machining on the quality of the surface generated on a carbon fibre reinforced polymer composite, *Machines*, Vol. 11, pp. 749.

[25] KARTHIK, K., SUNDARSINGH, D. S., HARIVIGNESH, M., KARTHICK, R. G., PRAVEEN, M. (2021). Optimization of machining parameters in abrasive water jet cutting of stainless steel 304. *Mater. Today Proc*, Vol. 46, pp. 1384-1389.

[26] NAG, A., DIXIT, A. R., PETRŮ, J., VÁŇOVÁ, P., KONEČNÁ, K., HLOCH, S. (2024). Maximization of wear rates through effective configuration of standoff distance and hydraulic parameters in ultrasonic pulsating waterjet. *Facta Univ., Ser.: Mech. Eng*, Vol. 22, No. 2, pp. 165–186.

[27] LISSEK, F., KAUFELD, M., TEGAS, J., HLOCH, S. (2016) . Online-monitoring for abrasive waterjet cutting of CFRP via acoustic emission: evaluation of machining parameters and work piece quality due to burst analysis. *Procedia Eng*, Vol.149 , pp. 67–76.

[28] SHARMA, V., CHATTOPADHYAYA, HLOCH, S. (2011) . Multi response optimization of parameters based on Taguchi-Fuzzy model for coal cutting by water jet technology. *Int. J. Adv. Manuf. Technol*, Vol. 56, pp. 1019–1025.

[29] NAG, A., SRIVASTAVA, A. K., DIXIT, A. R. (2017) . Influence of abrasive water jet turning parameters on variation of diameter of hybrid metal matrix composite, *Applications of Fluid Dynamics: Proceedings of ICAFD 2016*, pp. 495–504.

[30] GANOVSKA, B., MOLITORIS, M., HOSOVSKY, A., PITEL, J., KROLCZYK, J. B., RUGGIERIO, A., KROLCZYK, G. M., HLOCH, S. (2016). Design of the model for the on-line control of the AWJ technology based on neural networks. *Indian Journal of Engineering & Materials Sciences*, Vol.23, pp. 279-287.

[31] LEI, Y. Y., TANG, P. H., JIANG, D. J., LIU, K. F. (2010). Artificial neural network model of abrasive water jet cutting stainless steel process. *Proc of IEEE Int Conf on Mechanic Automation and Control Engineering (MACE)*, pp. 3507-3511.

[32] YANG, G. L. (2013). Forecast surface quality of abrasive water jet cutting based on neural network. *Journal of Theoretical and Applied Information Technology*, Vol. 47, No. 3, pp. 1087-1091.

[33] HREHA, P., HLOCH, S., PERŽEL, V. (2012). Analysis of acoustic emission recorded during monitoring of abrasive waterjet cutting of stainless steel AISI 309. *Tehnicki Vjesnik-Technical Gazette*, Vol. 19, No. 2, pp. 355-359.

[34] HASHISH, M., LOSCUTOFF, W. V., REICH, P. (1983). Cutting with abrasive water jets. *Proeedings of the Second U.S Water jet conference*, pp. 65-66.

[35] MOMBER, A. W. (1995). A generalized abrasive water jet cutting model. *Labus TJ(ed) 1995 Proc.8th Amer.Wter Jet Conf.*, Vol.1, pp. 359-371.